Langmuir Article

pubs.acs.org/Langmuir

Perturbation Solution of the Shape of a Nonaxisymmetric Sessile Drop

Bharadwaj Prabhala,[†] Mahesh Panchagnula,*[,†] Venkat R. Subramanian,[‡] and Srikanth Vedantam[§]

[†]*Departmental of Mechanical Engineering, Tennessee Technological University, Cookeville, Tennessee 38505,* [‡]*Department of Energy, Environmental and Chemical Engineering, Washington University, St. Louis, Missouri 63130, and* [§]*Departmental of Mechanical Engineering, National University of Singapore, Singapore*

Received November 10, 2009. Revised Manuscript Received May 13, 2010

We develop an approximate analytical solution for the shape of a nonaxisymmetric sessile drop using regular perturbation methods and ignoring gravity. We assume that the pinned, contorted triple-line shape is known and is a small perturbation of the circular footprint of a spherical cap. We obtain an analytical solution using regular perturbation methods that we validate by comparing to the numerical solution of the Young−Laplace equation obtained using publicly available Surface Evolver software. In this process, we also show that the pressure inside the perturbed drop is unchanged and relate this to the curvature of the drop using the Young−Laplace equation. The rms error between the perturbation and Evolver solutions is calculated for a range of contact angles and amplitudes of triple-line perturbations. We show that the perturbation solution matches the numerical results well for a wide range of contact angles. In addition, we calculate the extent to which the drop surface is affected by triple-line contortions. We discuss the applicability of this solution to the possibility of real time hybrid experimental/computational characterization of the 3D sessile drop shapes, including obtaining local contact angle information.

1. Introduction

Sessile drops are characterized by the angle between the liquid−vapor interface and the solid−liquid surface at the solid−liquid−vapor triple line. This angle, known as the contact angle, is determined by the relative magnitudes of the liquid−solid and liquid−vapor interfacial energies. Drops on ideal, rigid, flat, and homogeneous surfaces take the shape of a spherical cap (in the absence of gravity) with perfectly circular triple lines and constant contact angles. On real surfaces, the triple lines are pinned into contorted shapes and the wrinkles spread to the surface of the spherical cap, resulting in a variation of the local contact angle around the periphery. The pinning of the triple line at heterogeneities and the local contact angle along the contorted triple line determine the local wetting/dewetting characteristics of the drop, particularly the contact angle hysteresis.[1] It is thus necessary to determine the 3D shapes of drops on real heterogeneous surfaces.

Previous studies of the wetting characteristics of heterogeneous surfaces have employed 3D simulations of the drop.[2,3] However, recognizing that the triple-line interactions with heterogeneities determine the drop contact behavior,[4,5] Vedantam and Panchagnula[6,7] have proposed a 2D approach (based on the average contact angle of the sessile drop) that focuses purely on the triple line and its interactions with heterogeneities on the solid surface. One of the stated purposes of the full numerical simulations is to determine the local contact angle on the triple line because the local advancing/receding behavior is influenced by this parameter. The local contact angle can be calculated from the 3D shape of the drop subject to the pinned triple-line shape.[8] Several previous studies of numerical computations of 3D drop shapes have been performed using the Surface Evolver program.[2,9,10] However, such simulations are computationally intensive and have been restricted to the calculation of drop shapes on relatively simple patterns of heterogeneities. In this article, we propose an alternative, approximate analytical solution of the nonaxisymmetric drop shape with a generally contorted triple line based on the regular perturbation method.

The 3D shape of sessile drop surface is governed by the Young−Laplace equation,[4] which relates the capillary pressure difference sustained across an interface separating two static fluids to the local mean curvature, κ,

$$P_i - P_o = \sigma\kappa \tag{1}$$

Here, P_i is the local pressure within the drop, P_o is the atmospheric pressure, and σ is the surface tension of the liquid. In the case of small sessile drops, gravity can be neglected and P_i and P_o are both constant. The Young−Laplace equation (eq 1) thus indicates that the liquid−vapor surface has a constant mean curvature.

In the presence of pinning heterogeneities, the surfaces of sessile drops become wrinkled. However, the Young−Laplace equation still holds true for the drops in the pinned condition, and the mean curvature of the liquid−vapor interface is constant in the absence of gravity. Using this and the fact that the wrinkled drop is a

(1) Decker, E. L.; Garoff, S. Contact line structure and dynamics on surfaces with contact angle hysteresis. *Langmuir* **1997**, *13*, 6321−6332.
(2) Marmur, A. Contact angle hysteresis on heterogeneous smooth surfaces. *J. Colloid Interface Sci.* **1994**, *168*, 40−46.
(3) Kusumaatmaja, H.; Yeomans, J. M. Modeling contact angle hysteresis on chemically patterned and superhydrophobic surfaces. *Langmuir* **2007**, *23*, 6019−6032.
(4) deGennes, P. G.; Brochard-Wyart, F.; Quere, D. *Capillarity and Wetting Phenomena*; Springer: New York, 2002.
(5) Panchagnula, M. V.; Vedantam, S. Comment on How Wenzel and Cassie were wrong by Gao and McCarthy. *Langmuir* **2007**, *23*, 13242−13242.
(6) Vedantam, S., Panchagnula, M. V. Phase field modeling of hysteresis in sessile drops. *Phys. Rev. Lett.* **2007**, *99*, 176102.
(7) Vedantam, S., Panchagnula, M. V. Constitutive modeling of contact angle hysteresis. *J. Colloid Interface Sci.* **2008**, *321*, 393−400.
(8) Marmur, A. Solid-surface characterization by wetting. *Annu. Rev. Mater. Res.* **2009**, *39*, 473−489.
(9) Brandon, S.; Wachs, A.; Marmur, A. Simulated contact angle hysteresis of a three-dimensional drop on a chemically heterogeneous surface: a numerical example. *J. Colloid Interface Sci.* **1997**, *191*, 110−116.
(10) Iliev, S.; Pesheva, N. Nonaxisymmetric drop shape analysis and its application for determination of the local contact angles. *J. Colloid Interface Sci.* **2006**, *301* 677−684.

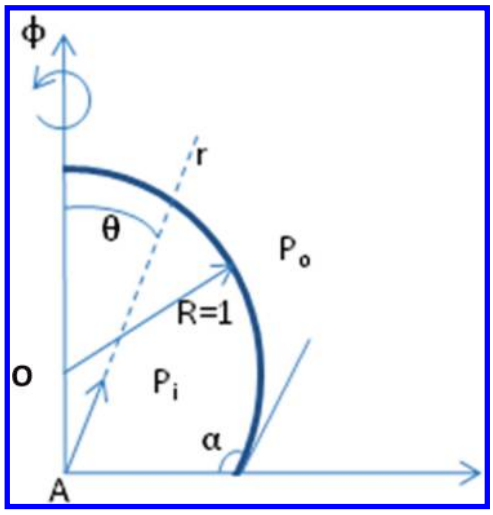

Figure 1. Schematic representation of a sessile drop.

perturbation of the axisymmetric drop, we develop a perturbation solution to predict the shape of the sessile drop for a generally nonaxisymmetric pinned triple line. We validate the analytical solution by comparing the drop shapes for the same triple-line topology and drop volume to the numerical solution of the exact Young−Laplace equation obtained using public domain Surface Evolver software.[11] Finally, using the analytical solution, we investigate the dependence of the local contact angles on the configuration of the triple-line shape of a sessile liquid drop on a solid substrate. An extensive parametric study is also conducted by varying the contact angle that the drop makes with the solid substrate and the amplitude of the triple-line contortions in order to ascertain the domain of applicability of the analytical solution. We find that the perturbation approach matches the numerical computation well for a wide range of contact angles and pinning strengths of the heterogeneities. Finally, we determine the extent to which the drop surface is affected by the contortions on the triple line.

2. Theory

In this section, we summarize the development of the perturbation solution for the shape of the sessile drop. The analytical solution is based on a perturbation expansion of the mean curvature subject to a contorted pinned triple line.

Consider a drop exhibiting a contact angle α while sessile on an ideal (defect-free) surface as shown in Figure 1. Let A be the origin, θ be the zenith angle, and φ be the azimuthal angle. Let O be the geometric center of the sphere that the drop is part of. Let the pressure inside and outside the drop be P_i and P_o, respectively. Without a loss of generality, we assume that the drop in the unperturbed state is the unit radius.

In the case of the drop on an ideal surface, the triple line is a circle with radius of sin α given by the equation

$$r = \sin\alpha;\ \theta = \frac{\pi}{2} \tag{2}$$

The unperturbed surface of the sessile drop is a part of a sphere that in the chosen coordinate system can be expressed by the equation

$$f_u(r,\theta,\varphi):\ r - F(\theta) = 0 \tag{3}$$

where

$$F(\theta) = \sqrt{\cos^2\theta\cos^2\alpha + \sin^2\alpha} - \cos\theta\cos\alpha \tag{4}$$

It may be noted that the volume of the unperturbed drop, V_u, enclosed by this surface is given by

$$V_u = \int_0^{2\pi}\int_0^{\pi/2}\int_0^{F(\theta)} r^2\,dr\sin(\theta)\,d\theta\,d\varphi = \int_0^{2\pi}\int_0^{\pi/2}\frac{F^3}{3}\sin\theta\,d\theta\,d\varphi \tag{5}$$

With $F(\theta)$ given by eq 4, it can be shown using MAPLE that the volume of the unperturbed drop is the same as that of the spherical cap given by

$$V_u = \frac{\pi}{3}(\cos^3\alpha - 3\cos\alpha + 2) \tag{6}$$

The unit normal vector $\hat{n}_u$ on this surface is given by

$$\hat{n}_u = \frac{\nabla f_u}{|\nabla f_u|} = \frac{F\hat{e}_r - F_\theta\hat{e}_\theta}{\sqrt{F^2+F_\theta^2}} \tag{7}$$

where subscript θ on F denotes differentiation. The curvature κ_u of the drop is calculated by taking the divergence of the normal vector $\hat{n}_u$ that is given by the following equation:

$$\kappa_u = \nabla\hat{n}_u \tag{8}$$

Using eq 5, the curvature κ_u is given explicitly by

$$\kappa_u = \frac{1}{F\sin\theta\sqrt{F^2+F_\theta^2}}\left[2F\sin\theta - F_\theta\cos\theta + \sin\theta\left(\frac{FF_\theta^2 - F_{\theta\theta}F^2}{F^2+F_\theta^2}\right)\right] \tag{9}$$

Upon simplifying eq 9 using eq 4, we note that the value of κ_u is 2 for any value of θ and α, as is to be expected for the unit sphere. So far we have considered the unwrinkled spherical cap to be the drop surface. We now consider a situation in which the triple line is pinned in a contorted configuration because of heterogeneities on the surface. We will assume that the contorted triple line can be described by

$$r = \sin\alpha(1+\varepsilon g(\varphi));\ \theta = \frac{\pi}{2} \tag{10}$$

where g(φ) (of order 1) is assumed to be a periodic function of φ and ε is the (small) amplitude of perturbation from the ideal contact circle radius given by eq 2. For this perturbed triple line, let the 3D perturbed surface be given by

$$f_p(r,\theta,\varphi):\ r - (F(\theta) + \varepsilon G(\theta,\varphi)) = 0 \tag{11}$$

This ansatz is the most general form in which the triple-line contortions contribute to O(ε) wrinkling of the surface. That is, the O(ε) contortions of the triple line do not affect the O(1) spherical cap shape of the drop in keeping with a regular perturbation expansion. We note that this choice is the same as

(11) Brakke, K. A. *The Surface Evolver*; **1992**.

in Popova[12] and Myshkis et al.,[13] who have both presented a similar regular perturbation solution for the shape of the non-axisymmetric drop, albeit restricted to the case of $\alpha = 90°$.

The unit normal vector $\hat{n}_p$ on this perturbed surface can be evaluated just as was done for the unperturbed surface. Retaining the terms in $\hat{n}_p$ only up to order ε, we may write

$$\hat{n}_p = \frac{F\hat{e}_r - F_\theta \hat{e}_\theta}{\sqrt{F^2+F_\theta^2}} + \frac{\varepsilon}{\sqrt{F^2+F_\theta^2}}\left[\frac{F_\theta}{F^2+F_\theta^2}\{-G_\theta F + GF_\theta\}\hat{e}_r - \frac{(G_\theta F^2 + GFF_\theta)}{F^2+F_\theta^2}\hat{e}_\theta - \frac{G_\varphi}{\sin\theta}\hat{e}_\varphi\right] + O(\varepsilon^2) \quad (12)$$

The curvature κ_p of the perturbed surface is once again evaluated by finding the divergence of the normal vector, $\hat{n}_p$

$$\kappa_p = \nabla \hat{n}_p \quad (13)$$

Again, by retaining the $O(\varepsilon)$ terms, we find that κ_p is of the form

$$\kappa_p = \kappa_u + \varepsilon(f_1(\theta)G_{\theta\theta} + f_2(\theta)G_\theta + f_3(\theta)G_{\varphi\varphi}) + O(\varepsilon^2) \quad (14)$$

From the Young−Laplace equation (eq 1), if P_i' is the (constant) pressure within the perturbed drop and P_o is the atmospheric pressure, then it follows that

$$P_i' - P_o = \sigma\kappa_p \quad (15)$$

First, it can be seen from the above that because P_i' is constant within the drop, κ_p does not depend on θ and φ. This implies that the $O(\varepsilon)$ term on the right-hand side of eq 14 is at most a function of α. Therefore,

$$\kappa_p = \kappa_u + \varepsilon C(\alpha) + O(\varepsilon^2) \quad (16)$$

with $C(\alpha)$ as yet undetermined. Second, we calculate the perturbed surface such that the perturbed and unperturbed drops have the same volume. In this regard, the volume enclosed by the perturbed surface is given by

$$V_p = \int_0^{2\pi}\int_0^{\pi/2}\int_0^{(F+\varepsilon G)} r^2\, dr \sin\theta\, d\theta\, d\varphi \quad (17)$$

and the perturbed drop surface is given by eq 11 and hence the upper limit of the innermost integral. By retaining terms up to $O(\varepsilon)$, we may write

$$V_p = \int_0^{2\pi}\int_0^{\pi/2}\frac{F^3}{3}\sin(\theta)\, d\theta\, d\varphi + \varepsilon\int_0^{2\pi}\int_0^{\pi/2} F^2 G \sin(\theta)\, d\theta\, d\varphi + O(\varepsilon^2) \quad (18)$$

Using eq 16 together with eq 14, we find that

$$f_1(\theta)G_{\theta\theta} + f_2(\theta)G_\theta + f_3(\theta)G_{\varphi\varphi} = C(\alpha) \quad (19)$$

This is the governing equation for $G(\theta, \varphi)$, and the forms of functions $f_i(\theta)$ ($i = 1, 2, 3$) are included in the Appendix. The boundary conditions for $G(\theta, \varphi)$ are

$$G(\theta,0) = G(\theta,2\pi);\ G_\varphi(\theta,0) = G_\varphi(\theta,2\pi);$$
$$G_\theta(0,\varphi) = 0;\ G_\varphi\left(\frac{\pi}{2},\varphi\right) = g(\varphi) \quad (20)$$

The solution of $G(\theta, \varphi)$ can be separated into particular and homogeneous solutions such that

$$G(\theta,\varphi) = G^{(p)}(\theta) + G^{(h)}(\theta,\varphi) \quad (21)$$

where $G^{(p)}(\theta)$ is allowed to satisfy the equation

$$f_1(\theta)G^{(p)}_{\theta\theta} + f_2(\theta)G^{(p)}_\theta = C(\alpha) \quad (22)$$

subject to the conditions

$$G^{(p)}_\theta(0) = 0;\ G^{(p)}\left(\frac{\pi}{2}\right) = 0 \quad (23)$$

and $G^{(h)}(\theta, \varphi)$ satisfies the homogeneous version of eq 19 given by

$$f_1(\theta)G^{(h)}_{\theta\theta} + f_2(\theta)G^{(h)}_\theta + f_3(\theta)G^{(h)}_{\varphi\varphi} = 0 \quad (24)$$

subject to the boundary conditions

$$G^{(h)}(\theta,0) = G^{(h)}(\theta,2\pi);$$
$$G^{(h)}_\varphi(\theta,0) = G^{(h)}_\varphi(\theta,2\pi);$$
$$G^{(h)}_\theta(0,\varphi) = 0;\ G^{(h)}\left(\frac{\pi}{2},\varphi\right) = g(\varphi) \quad (25)$$

A solution to eq 22 subject to eqs 23 can be written using the method of variation of parameters after defining a function $\psi(0) = \exp[-\int (f_2/f_1)\, d\theta]$. This solution takes on the form

$$G^{(p)}(\theta) = C(\alpha)\left\{C_1 + C_2\int \psi\, d\theta + \int\frac{\int\psi\, d\theta}{\psi}d\theta + \left(\int\psi d\,\theta\right)\left(\int\frac{d\theta}{\psi}\right)\right\} = C(\alpha)\, H(\theta,\alpha)(\text{say}) \quad (26)$$

where C_1 and C_2 are determined from eqs 23.We will now turn our attention to the solution of eq 24 subject to the first three boundary conditions of eqs 25 using the method of separation of variables in order to develop an analytical solution for $G^{(h)}(\theta, \varphi)$.

$$G^{(h)}(\theta,\varphi) = T(\theta)\, P(\varphi) \quad (27)$$

Substituting eq 27 into eq 19 yields

$$\frac{f_1(\theta)T'' + f_2(\theta)T'}{f_3(\theta)T} = -\frac{P''}{P} = +\lambda^2 \quad (28)$$

Here, the prime denotes differentiation with respect to its argument and λ^2 is the separation constant in the usual sense. The equation for $P(\varphi)$ constitutes an eigenvalue problem with sine and cosine functions being independent solutions,

$$P_m(\varphi) = A_m^{(s)}\sin(m\varphi) + A_m^{(c)}\cos(m\varphi) \quad (29)$$

(12) Popova, L. N., Nonaxisymmetric equilibrium shapes of a drop on a plane. *Fluid Dyn.* **1983**, *18*, 634−637.
(13) Myshkis, A. D.; Babskii, V. G.; Kopachevskii, N. D.; Slobozhanin, L. A.; Tyuptsov, A. D. *Low Gravity Fluid Mechanics*; Springer-Verlag: Berlin, 1987.

Here $m = 1, 2, 3...$ (the set of nonzero integers) are the corresponding eigenvalues that arise from the periodicity condition in eq 20 and $A_m^{(s)}$ and $A_m^{(c)}$ are still arbitrary constants whose values need to be determined to satisfy the fourth boundary condition of eq 20. Because $m = 1$ represents a rigid translation of the drop (for small ε), we consider only the $m > 1$ case. Corresponding to each $m > 1$, the equation for $T_m(\theta)$ constitutes a boundary value problem

$$f_1(\theta)T_m'' + f_2(\theta)T_m' - m^2 f_3(\theta)T_m = 0;\ 0 < \theta < \frac{\pi}{2} \tag{30}$$

with the boundary conditions

$$T_m\left(\frac{\pi}{2}\right) = 1 \text{ and } T_m'(0) = 0 \tag{31}$$

By solving eqs 30 subject to eqs 31, we obtain the complete solution for $G^{(h)}(\theta, \varphi)$ and therefore $G(\theta, \varphi)$ as

$$G(\theta,\varphi) = C(\alpha)\,H(\theta,\alpha) + \sum_{m=1}^{\infty} T_m(\theta)(A_m^{(s)}\sin(m\varphi) + A_m^{(c)}\cos(m\varphi)) \tag{32}$$

The perturbation part of the triple line given by eq 10 can be written in terms of eigenfunctions $\sin(m\varphi)$and $\cos(m\varphi)$ as

$$g(\varphi) = \sum_{m=1}^{\infty} B_m^{(s)}\sin(m\varphi) + B_m^{(c)}\cos(m\varphi) \tag{33}$$

Here $B_m^{(s)}$ and $B_m^{(c)}$ are the Fourier coefficients that describe the perturbations on the triple line. By imposing the fourth boundary condition in eq 25 on the solution in eq 32, it can readily be seen that $A_m^{(c)} = B_m^{(c)}$ and $A_m^{(s)} = B_m^{(s)}$ because $H(\pi/2, \alpha) = 0$ from the second condition in eq 23. The solution in eq 32 is now fully determined except for the function $C(\alpha)$. We now turn to determining $C(\alpha)$. Using eq 5, we can rewrite eq 18 as

$$V_p = V_u + \varepsilon\int_0^{2\pi}\int_0^{\pi/2} F^2\,G\sin(\theta)\,d\theta\,d\varphi + O(\varepsilon^2) \tag{34}$$

By using eq 32 for $G(\theta, \varphi)$ and realizing that $G^{(h)}$ is in a separable form, eq 34 becomes

$$V_p = V_u + 2\pi\varepsilon C(\alpha)\int_0^{\pi/2} F^2 H\sin\theta\,d\theta + \varepsilon\sum_{m=1}^{\infty}\left\{\int_0^{\pi/2} F^2 T_m(\theta)\sin\theta\,d\theta\left[A_m^{(s)}\int_0^{2\pi}\sin(m\varphi)\,d\varphi + A_m^{(c)}\int_0^{2\pi}\cos(m\varphi)\,d\varphi\right]\right\} + O(\varepsilon^2) \tag{35}$$

The term inside the square brackets is identically zero for all m, which implies that

$$V_p = V_u + 2\pi\varepsilon C(\alpha)\int_0^{\pi/2} F^2 H\sin\theta\,d\theta + O(\varepsilon^2) \tag{36}$$

It may be recalled that we require $V_p = V_u + O(\varepsilon^2)$. In addition, it was verified numerically that $\int_0^{\pi/2} F^2 H\sin\theta\,d\theta \neq 0$ in general for all α. Therefore, we conclude that $C(\alpha) \equiv 0$ and the solution for $G(\theta, \varphi)$ is given by

$$G(\theta,\varphi) = \sum_{m=1}^{\infty} T_m(\theta)(B_m^{(s)}\sin(m\varphi) + B_m^{(c)}\cos(m\varphi)) \tag{37}$$

Because the boundary value problem given by eqs 30 and 31 does not have a general analytical solution, a 15-term series solution developed in MAPLE is therefore used as an approximation. It must be mentioned that for the special case of $\alpha = \pi/2$, eqs 30 reduce to the associated Legendre equation. The solutions for $T_m(\theta)$ for this special case are the associated Legendre functions of the first kind. For any other α, the series $T_m(\theta)$ can be construed as a generalized associated Legendre function of the first kind.

3. Numerical Solution

The analytical solution given by eq 32 is validated using the surface shape calculated using a numerical solution of the Young−Laplace equation. We use open source program Surface Evolver for this purpose. Surface Evolver is an interactive program for the study of the evolution of surfaces that are shaped by surface tension and other energies. The algorithm calculates the velocity of each vertex, and the vertex is moved in the direction such that the surface evolves toward a minimum energy by the gradient descent method. Thus, the final equilibrium shape is calculated following a series of energy-minimizing successive approximations starting from an initial state. More details of the algorithm and the program implementation can be found in the user manual.[14]

For a given shape of the triple line such as that given in eq 10 and the drop volume, the drop shape is computed using Surface Evolver. The initial shape with which we start the evolution of the drop is a pyramid, with the base forming the triple line given by eq 10. The vertices and edges that form the triple line are constrained to remain on the $\theta = \pi/2$ plane and are rendered immobile. During the process of evolution through refinement, the drop shape is allowed to evolve into the final equilibrium shape subject to the constraints of constant volume and an immobile triple line. For the purpose of validating the analytical solution, we begin with a simple form of $g(\varphi)$ in eq 33 given by

$$g(\varphi) = \sin(n\varphi) \tag{38}$$

The mean contact angle that the drop makes with the substrate (α), the number of undulations (n), and the amplitude of undulations (ε) are the parameters in this problem. For a given grid (number of facets), the Surface Evolver iteration process was allowed to progress until convergence was achieved to 12 significant digits. In addition, the number of facets used to approximate the surface is also gradually increased (using the refinement feature) from about 4000 to about 66 000 facets (or more) until the converged energies from successively refined grids differed only in the sixth significant digit. At this point, a grid-independent solution was thought to have been realized. It may be noted that the sequence of operations employed was the same for all cases but the number of iterations required for the solution to reach complete convergence was different for different cases of n and ε.

The grid-independent Surface Evolver solution was used to validate the perturbation solution. For purposes of comparison, the total rms error in the radii at all vertex locations between the analytical and numerical solutions was calculated. This process

(14) Brakke, K. *Surface Evolver User's Manual*; **2008**.

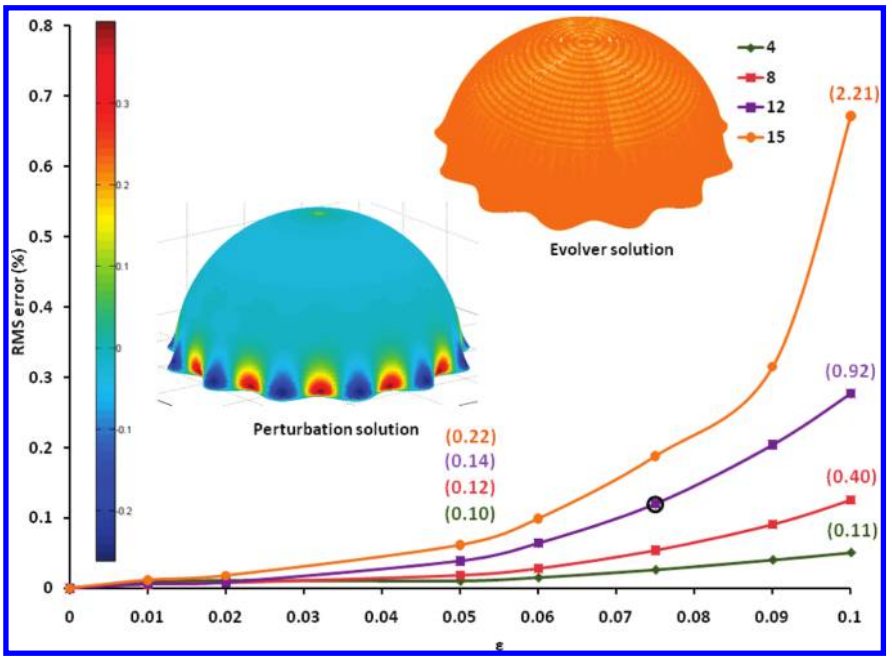

Figure 2. Plot of rms error vs ε for different n values and a contact angle of 90°. The inset images correspond to the circled data point.

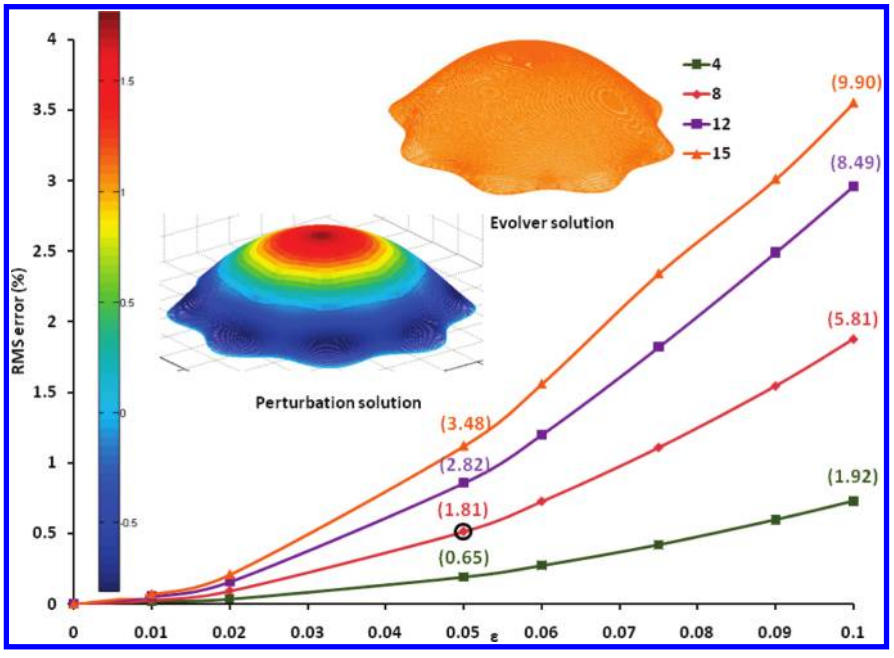

Figure 3. Plot of rms error vs ε for different n values and a contact angle of 45°. The inset images correspond to the circled data point.

involves extracting information on the coordinates of all of the vertices from the Surface Evolver solution in a Cartesian coordinate system and transforming it into a spherical polar system in which the analytical solution is available. With a knowledge of θ and φ at each vertex from the Surface Evolver solution, we compute the value of the radius from the analytical solution for θ and φ, With the value of the radius at each vertex obtained through both the analytical and Surface Evolver solutions, the rms error is calculated over all of the vertex points and presented as a ratio with the mean radius of the drop.

4. Results and Discussion

A parametric study was conducted using the analytical and Surface Evolver solutions to quantify the variation of the rms error as a function of the mean contact angle that the drop makes with the substrate (α), the number of undulations (n), and the amplitude of undulations (ε). Figures 2−4 depict the variation of the rms error with ε for different α and n.

Figure 2 represents the plot between the rms error versus ε for four different values of n (= 4, 8, 12, and 15) for $\alpha = 90°$. It can be seen from the graph that the rms error increases with increasing triple-line undulation amplitude (ε) as well as with the number of undulations (n). It can also be observed from this graph that the difference between the Surface Evolver and analytical solutions reaches a maximum value of 0.7% for $\varepsilon = 0.1$ and $n = 15$. The maximum local error in percentage terms for the four values of n is indicated in parentheses for $\varepsilon = 0.05$ and 0.1. The inset images in the plot show the 3D shape of the drop obtained from the Surface Evolver and analytical approaches for the case of $n = 12$ and

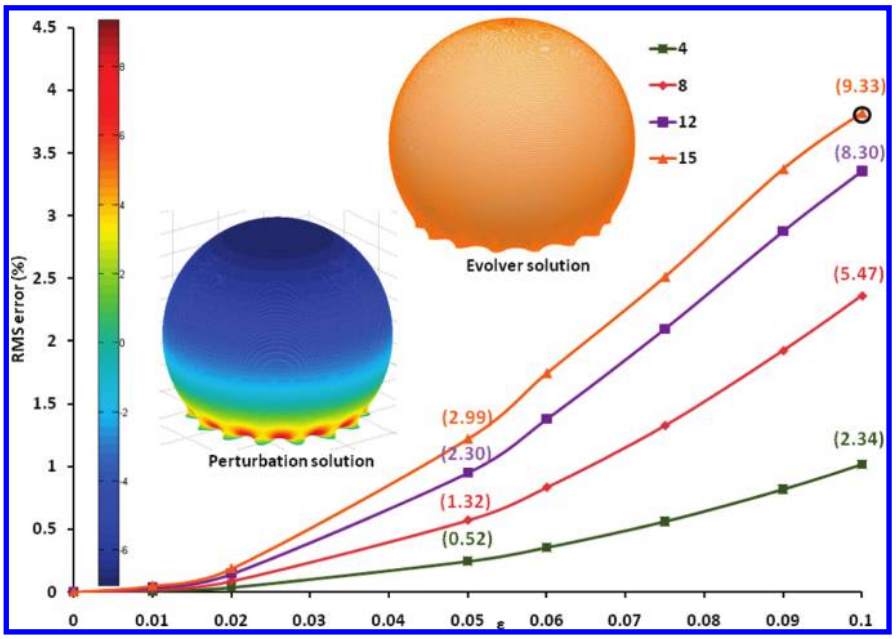

Figure 4. Plot of rms error vs ε for different n values and a contact angle of 135°. The inset images correspond to the circled data point.

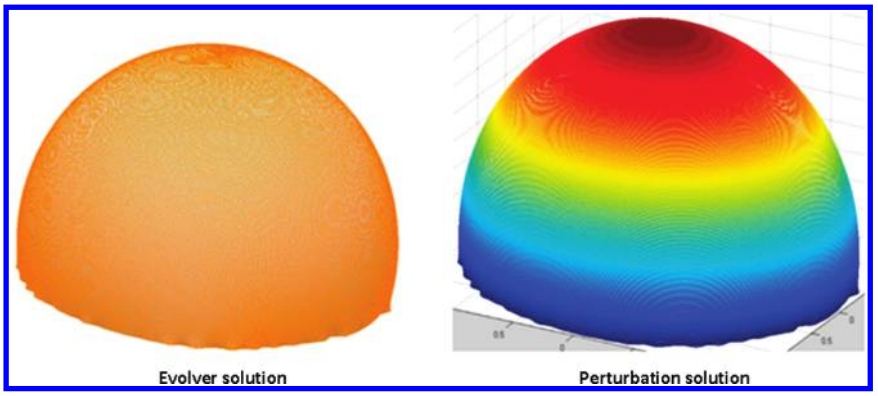

Figure 5. Drop shapes obtained from numerical and analytical solutions for a real triple line.

$\varepsilon = 0.075$. The perturbation solution is shown in pseudocolor with the color scale indicating the local error in percentage terms. First, it can be seen that the shapes of the drop obtained from both approaches are almost identical. Second, the maximum local error occurs in the region above the contact line. Third, from the maximum errors, for $\varepsilon = 0.1$ the maximum error is only 2.21%. Therefore, it can be concluded that the approximate analytical solution has been validated. Furthermore, it must be mentioned that the numerical solution took approximately 6 min on a 2.2 GHz processor whereas the analytical solution is obtained in 5 s.

Figures 3 and 4 represent plots similar to Figure 2 for the cases of $\alpha = 45$ and 135°, respectively. The qualitative trends in the variation of the rms error versus ε and n are similar to those in Figure 2. However, the maximum rms errors for $\alpha = 45$ and 135° are 3.7 and 4%, respectively, which are both higher than for $\alpha = 90°$. On each of these two figures, a comparison is provided between the exact and perturbation solutions for one data point, which is circled. It can be observed from these images that the local error for the 45° case is highest at the top of the drop whereas for the 135° case the local errors are high near the contact line. In addition, the maximum local errors for $\varepsilon = 0.05$ and 0.1 are also indicated on the Figure. The maximum local error is on the order of ε for this case. The perturbation solution drop shapes are colored by the local error according to the color bar shown in each graph.

In conclusion, the data in Figures 2−4 shows that the perturbation solution agrees well with the Surface Evolver solution. A primary benefit of the analytical approach lies in being able to calculate the local contact angle at any point on the triple line without needing to resort to the full numerical solution. In a typical experiment, it may be possible to measure the detailed shape of the triple line.[15,16] However, measuring the local contact angle is very difficult. This perturbation solution therefore presents a means to calculate the local contact angle for a given triple-line shape and drop volume.

Consider a situation of a small sessile drop (of radius smaller than the capillary length) of volume V. From the measurement of the triple line, it possible to calculate the average radius of the contact "circle". From these two measurements, it is possible to calculate the radius of the spherical cap R and the contact angle α. After the drop radius is nondimensionalized to unity, the analytical solution described by eq 32 is applicable. Coefficients $B_m^{(s)}$ and $B_m^{(c)}$ can be obtained from a Fourier transform (in the φ

(15) Bormashenko, E.; Bormashenko, Y.; Whyman, G.; Pogreb, R.; Musin, A.; Jager, R.; Barkay, Z. Contact angle hysteresis on polymer substrates established with various experimental techniques, its interpretation, and quantitative characterization. *Langmuir* **2008**, *24*, 4020−4025.

(16) Cubaud, T.; Fermigier, A. Advancing contact lines on chemically patterned surfaces. *J. Colloid Interface Sci.* **2004**, *269*, 171−177.

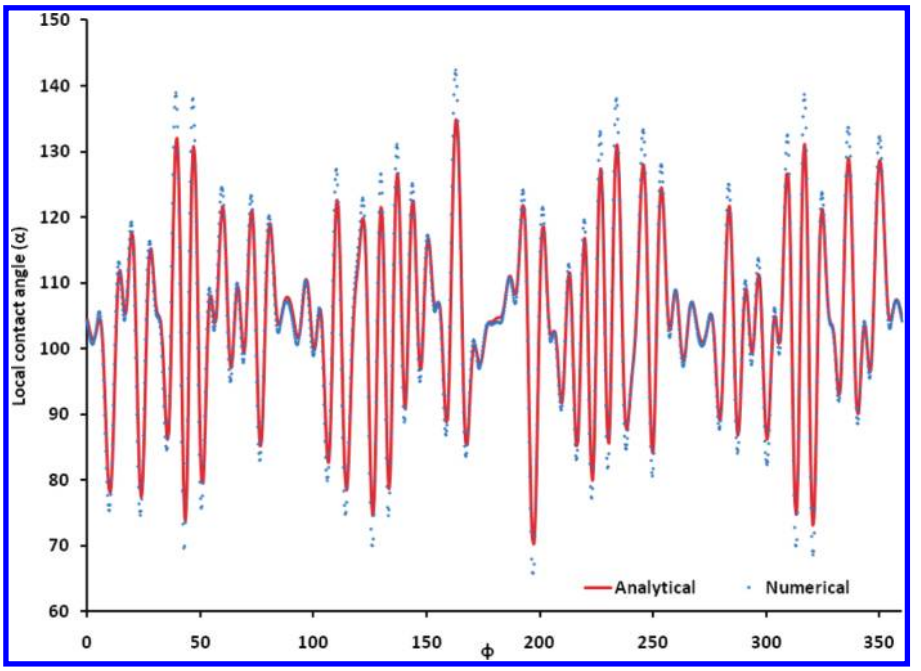

Figure 6. Plot of the local contact angle vs the azimuthal angle φ obtained from the Surface Evolver and the analytical solutions.

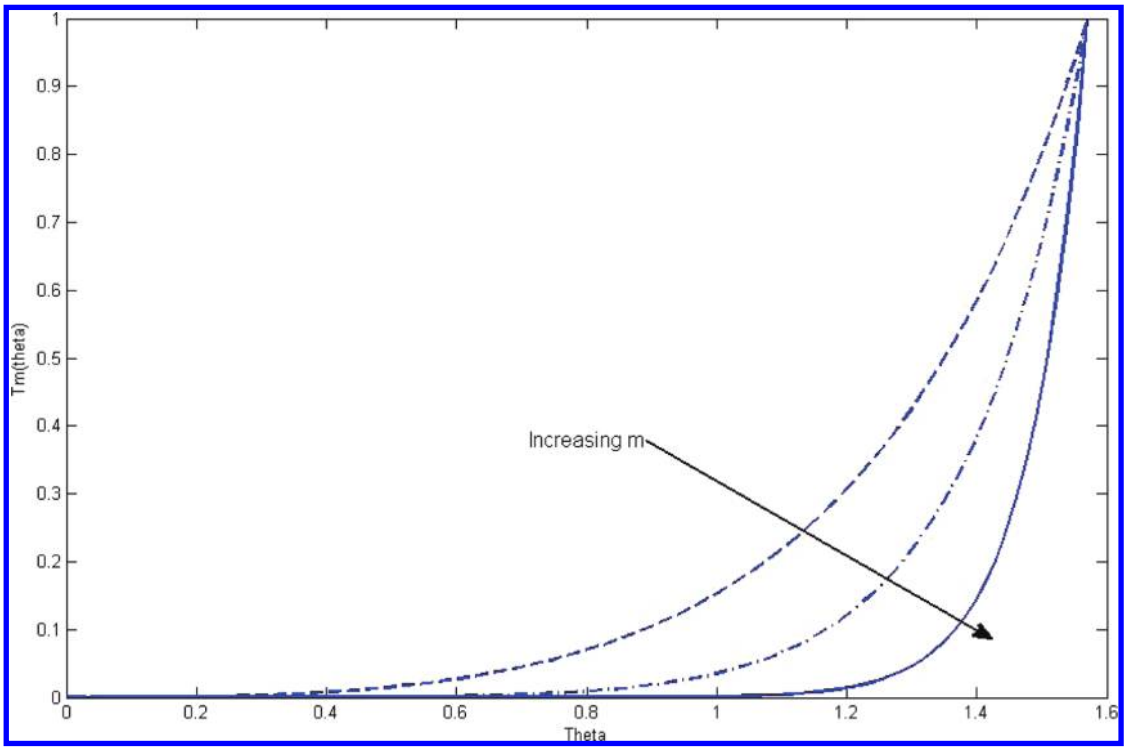

Figure 7. Plot of the variation of the amplitude of the triple-line contortion $T_m(\theta)$ as a function of the zenith coordinate θ. Note that $\theta = 0$ at the top of the drop.

coordinate) of the experimentally measured triple line. Presumably, the Fourier transform and the analytical solution computation can all be performed in approximately real time with some optimization and on a parallel machine resulting in real time 3D drop surface information. This can be realized from merely obtaining and analyzing a sequence of images of the triple line and knowledge of the drop volume. Such a hybrid theoretical/experimental approach has been proposed previously[10] and could serve to provide virtual 3D information in real time. In addition, the local contact angle information can yield information related to defect sites that adjoin and pin the triple line.

Figure 5 represents the comparison of the drop shape obtained by the Surface Evolver and analytical approaches for a sessile drop on a chemically heterogeneous substrate. The shape of the triple line was obtained from Anantharaju et al.,[17] who employed

(17) Anantharaju, N.; Panchagnula, M. V.; Vedantam, S. Asymmetric wetting of patterned surfaces composed of intrisically hysteretic materials. *Langmuir* **2009**, *25*, 7410−7415.

Table 1

serial no.	azimuthal wavenumber (m)	amplitude of perturbations (ε_m)
1	4	0.021
2	7	0.007
3	35	0.0068
4	27	−0.0066
5	15	0.0054
6	44	0.0054
7	40	−0.0053
8	17	0.0052
9	52	0.0052
10	56	−0.0046
11	9	0.0039
12	31	−0.0038
13	11	0.0036
14	25	−0.0031
15	30	−0.0007

phase field simulations of the advancing triple line on a substrate with square regions of a hydrophobic material of advancing angle 145° and receding angle 125° embedded in a hydrophilic material of advancing angle 95° and receding angle 83°. A Fourier analysis was performed on the triple-line shape of Figure 9 in Anantharaju et al.,[17] and only the 15 most significant terms were retained in eq 33. The values of n and ε for these 15 terms are listed in Table 1, along with the average contact angle, $\alpha = 104°$. The same triple-line shape was imposed as the boundary condition for both the analytical and Surface Evolver solutions. In addition, both calculations were carried out for the same drop volume, allowing us to compare these results. The rms error for this case is 4.03%.

Figure 6 is a plot of the local contact angle versus the azimuthal angle φ obtained from both Surface Evolver and the analytical solution. As can be seen, the agreement between the two is remarkable. Deviations between the two solutions are observed only where the contortions in the triple line are of very high frequency.

Figure 7 is a plot of $T_m(\theta)$ versus θ for $m = 3$, 5, and 10 and $\alpha = 120°$. This plot depicts the decay of the undulations introduced at the triple line. As can be seen from this plot, the higher-frequency contortions vanish closer to the triple line. For the case studied in Figure 5, it was found that for more than 90% of the drop surface area the drop shape remains within 1% of a spherical cap. This conclusion is qualitatively consistent with empirical observations of sessile drop surfaces in which even on significantly heterogeneous surfaces the drops seem to maintain their spherical cap shape, especially for larger contact angles.

5. Summary and Conclusions

An analytical solution based on a perturbation expansion was developed to predict the shape of the sessile drop (in the absence of gravity) for a given triple-line description. A numerical procedure was also developed in Surface Evolver to predict the 3D shape of the drop. A comparison between the analytical and numerical methods was made by calculating the rms error in the radius at all vertices of the Surface Evolver solution. Various test cases were run to check the validity of the analytical solution. The contact angles considered were 45, 90, and 135°. The number and amplitude of perturbations created on the triple line were varied for all three different contact angles. The calculation of the analytical solution is relatively much faster than the numerical solution, and the error between the two solutions is relatively low. The applicability of this solution to a hybrid experimental/computational investigation is discussed.

Appendix

The partial differential equation that governs the perturbation quantity $G(\theta, \varphi)$ is given by eq 19

$$f_1(\theta)G_\theta + f_2(\theta)G_\theta + f_3(\theta)G_{\varphi\varphi} = 0 \tag{19}$$

The forms of the functions $f_i(\theta)$ ($i = 1, 2, 3$) are included herein.

$$\begin{aligned} f_1(\theta) = {} & -2 + 2\cos^3\alpha\cos^3\theta\sqrt{\cos^2\theta\cos^2\alpha + \sin^2\alpha} \\ & - \cos\theta\cos^3\alpha\sqrt{\cos^2\theta\cos^2\alpha + \sin^2\alpha} \\ & + \cos\theta\cos\alpha\sqrt{\cos^2\theta\cos^2\alpha + \sin^2\alpha} \\ & - \cos^5\theta\cos^3\alpha\sqrt{\cos^2\theta\cos^2\alpha + \sin^2\alpha} \\ & - \cos^3\theta\cos\alpha\sqrt{\cos^2\theta\cos^2\alpha + \sin^2\alpha} + 3\cos^4\alpha\cos^2\theta \\ & - 3\cos^4\alpha\cos^4\theta - 4\cos^2\theta\cos^2\alpha + \cos^4\alpha\cos^6\theta \\ & + 2\cos^2\alpha\cos^4\theta + \cos^2\theta - \cos^4\alpha + 2\cos^2\alpha \end{aligned}$$

$$\begin{aligned} f_2(\theta) = {} & -4\sin\theta\cos^3\alpha\cos^2\theta\sqrt{\cos^2\theta\cos^2\alpha + \sin^2\alpha} \\ & - \sin\theta\cos\theta + 4\cos^4\theta\sqrt{\cos^2\theta\cos^2\alpha + \sin^2\alpha}\sin\theta\cos^3\alpha \\ & + \cos^2\theta\sin\theta\cos\alpha\sqrt{\cos^2\theta\cos^2\alpha + \sin^2\alpha} \\ & + 5\sin\theta\cos^2\alpha\cos\theta - 4\sin\theta\cos\theta\cos^4\alpha \\ & + 8\cos^3\theta\sin\theta\cos^4\alpha - 4\sin\theta\cos^4\alpha\cos^5\theta \\ & - 5\sin\theta\cos^3\theta\cos^2\alpha \end{aligned}$$

$$\begin{aligned} f_3(\theta) = {} & -1 + \cos\theta\cos\alpha\sqrt{\cos^2\theta\cos^2\alpha + \sin^2\alpha} \\ & - \cos^2\theta\cos^2\alpha + \cos^2\alpha \end{aligned}$$